Abstract

When light is shone onto complex media undergoing random motion, such as a colloidal suspension or biological tissue, a concave-up spike in the intensity distribution of the light scattered exactly back towards the source can be observed. This Coherent Backscattering (CBS) effect was first observed by Kuga in 1984. The relationship of the shape of the CBS spike, or cusp, to the optical properties of matter and optical phenomena was made clear by Albada and Lagendijk in 1985. Since then, there have been a few, but very sophisticated and expensive, experimental configurations aimed at recording the observation of the CBS effect. These setups have involved rare detection components such as cooled CCD cameras and photon-counting photomultiplier tubes, and expensive Argon-ion lasers. However, the effect can be observed using significantly less expensive equipment.

The aim of this study was to develop a novel method of analysis for detecting the coherent backscattering effect using a low cost experimental configuration. These observations could then be used to determine physical properties of the scattering medium.

A 10mW polarized HeNe laser, an AR-coated 50:50 cube beamsplitter, various convex lenses, a linear polarizer and an inexpensive CCD camera were used to detect light backscattered from samples of commercially available milk. The images exported by the CCD camera were analyzed using freely available Scion Image processing software, and the results clearly showed the concave-up intensity profiles whose shapes varied with the optical properties of the samples of milk. Theoretical fits to the data were then used to estimate light transport parameters, such as the root-mean free path length, of the scattering medium.

There are numerous plans to further extend the experimental configuration to allow observation in different polarization channels, develop more efficient methods of data analysis, and to implement the procedures in laboratory experiments.

1 Introduction

Light propagating through a randomly scattering medium towards its source is subject to interference effects. When light is shone onto complex media undergoing random motion, such as a suspension of colloidal particles or a photonic crystal in motion, a concave-up intensity spike can be observed in the light scattered back exactly towards the source. The appearance of this ordered, narrow, but well defined spike, or cusp is a fascinating and persistent phenomenon of light backscattered from a disordered scattering medium. This coherent backscattering (CBS) effect was first theorized and observed by Kuga in 1984 [1]. However, the relationship of the shape of the observed intensity spike to the the phenomenon of photon localization, or the enhanced probability for an incident photon to return to its starting point and reducing its propagation diffusion constant [3], and to the light transport parameters of the scattering medium [2] were not clear until later experiments had been conducted. CBS experiments have also been shown to have implications and applications in noninvasive imaging techniques, materials science research and mesoscopic physics [6].

Since CBS experiments involve the detection of low levels of scattered light, past experimental configurations to observe the effect have involved expensive equipment. Argon-ion lasers have been used as the light source, along with photon-counting photomultiplier tubes [4] and cooled CCD cameras [2] as detection mechanisms. Complicated off-centered rotational experimental setups [10] have also been implemented in order to measure the scattered light. However, the effect can be adequately measured using significantly less expensive components.

The aim of the present research was to observe the coherent backscattering effect from samples of ordinary milk by incorporating relatively inexpensive optical components in a CBS experimental setup, and by developing a novel method for analyzing the data gathered by the setup. A theoretical fit to these observations could be used to estimate the relative optical transport parameters of the samples. Further, such an experimental setup has research value to the optics laboratory and could be potentially useful to laboratory experiments.

Past studies involving the CBS of light have included gathering information about the structure of photonic crystals (including opals) [5], calculating the soil hot-spot effect in soils

composed of fine particles [7], estimating light transport parameters in biological media [2], and understanding light localization phenomena [11]. CBS of sunlight has also been observed and used to explain the narrow photometric effects from Saturn's rings [8].

After detecting and analyzing the scattered light, this theoretical fit to the observed CBS data was used to estimate the root-mean-free path length of light scattered inside ordinary samples of skim, 1%, and whole milk. These results then helped to characterize the different samples of milk by their optical properties.

2 Understanding Coherent Backscattering

Coherent backscattering can most easily be described by the model of planar waves scattering at multiple centers within a material, and self-interfering constructively at angles very close to 180°[4]. When the interference pattern has been averaged over multiple configurations, this constructive interference leads to the appearance of a narrow intensity cone centered at the exact backscattering direction. Figure 1 shows such a path, which a planar light wave and its time-reversed component could take through the scattering medium. CBS theory relates the width of these observed cone inversely to the root mean-free path that photons take within the complex scattering media.

2.1 CBS Theory

The quantity of interest in a CBS experiment is the average angular spread of the intensity of light backscattered by some randomly distributed scatterers undergoing some sort of random change in configuration, or a sort of ensemble averaging [6]. Examples of ideal samples include roughly spherical particles and emulsions in suspension, or complex solids undergoing some sort of motion. In such a situation (see Figure 1), the observed intensity distribution could be characterized as an averaging of the intensities observed from various pairs of plane waves and their momentum-reversed components, which are analogous to pairs of point source light. At the exact backscattered direction ($\theta = 0$), there is an enhancement since the interference between the plane waves and its counterpart is always constructive, leaving a cone shaped profile after averaging the observed intensities.

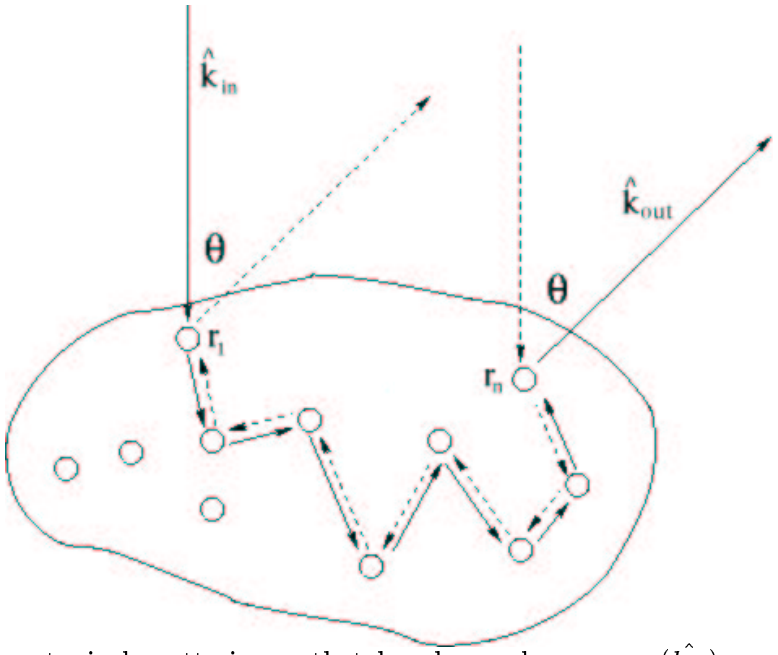

Figure 1: This is a typical scattering path taken by a plane wave ($\hat{k_{in}}$), and its time reversed component (represented by the dashed line). The phase difference between the plane wave and its component, ϕ, is the physical path length difference between the incoming and outgoing vectors, and can be represented by a function of the angle, θ, between them.

The phase difference between the incoming and outgoing light vectors, ϕ, for such systems as depicted in Figure 1 can be given by

$$\Delta\phi = \frac{2\pi}{\lambda}(\hat{k_j} + \hat{k_i}) \cdot (r_n - r_1)$$

where λ is the wavelength of the scattered light [6].

Using the photon diffusion approximation to determine the mean square distance between the first and last scatterers in randomly distributed scattering media, the final expression for the phase difference can be given as [4]

$$\Delta\phi \approx \frac{2\pi}{\lambda}\theta\sqrt{2l^*s}$$

where θ is the angle between the first and last scatterers, l^* is the transport mean-free scattering path length and s is the total scattering path length.

This phase expression yields a critical angle (θ_c), where if the two partial waves are in phase and the angle separating them is less than θ_c, then their amplitudes are added and squared to obtain the intensity; however, if they are out of phase, then their amplitudes

are squared then added to obtain the contributing intensity. This yields a theoretical enhancement factor of about 2 between the intensity observed at exactly 180°and some larger angle.

$$\theta_c \approx \frac{\lambda}{\sqrt{2l^* s}}$$

This expression for θ_c also indicates that the maximum angle at which any constructive interference occurs is inversely proportional to the mean path length, since at the maximum angular cone width, $s = l^*$.

Finally, the intensity profile can be derived within the diffusion approximation of scalar plane waves [4]:

$$I(q) = \frac{3}{16\pi}\left[1 + \frac{z_0}{l^*} + \frac{1}{(1+ql^*)^2}\left(1 + \frac{1-e^{-2qz_0}}{ql^*}\right)\right]$$

where $q = \frac{2\pi\theta}{\lambda}$ and $z_0 \approx \frac{2}{3}l^*$.

The function $I(q)$ given above for the intensity profile is essentially a lineshape curve for the intensity distribution. The variable q represents the angular distance from the exact backscattering direction, and is therefore always zero or positive. It is convenient to "fold over" the $I(q)$ function so that it better corresponds to the form of experimental data which are measured along some line passing through the 180°direction.

Figure 2 shows different lineshapes based on the parametrization by l^*. As the value used for l^* increases from 25 and 125 scattering events, to 625, the plotted cone becomes more and more narrow. The curve is one of the rare cases in which a function describing a phenomenon has a discontinuous derivative, or cusp.

It should be noted that the term in parenthesis in the above expression for $I(q)$,

$$\left(1 + \frac{1-e^{-2qz_0}}{ql^*}\right)$$

is typically very close to unity and can be neglected. This approximation was made when the theoretical function was matched to the experimental data.

Now discuss polariztion ... not too specific !

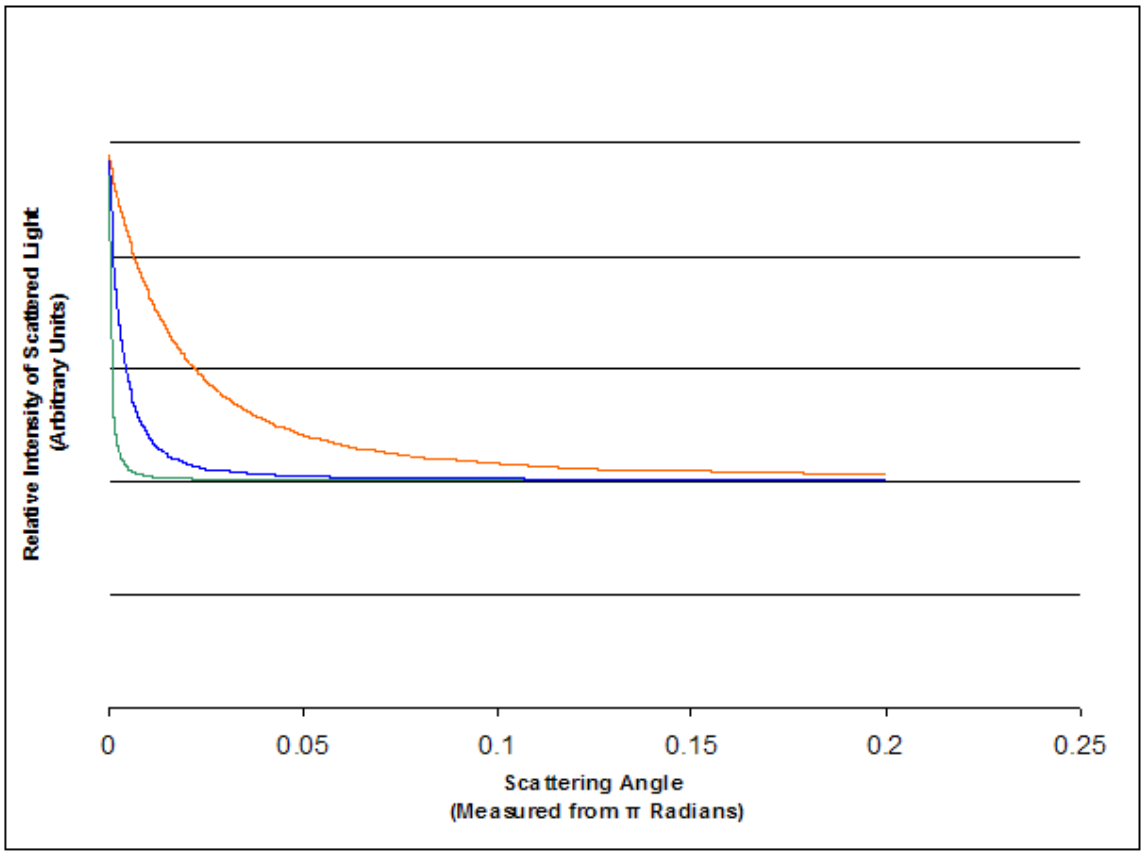

Figure 2: This graph shows three separate fits to the intensity profile lineshape expression using three different l^* values: 25 (Red), 125 (Blue) and 625 (Green) scattering events. It becomes clear that as the mean-free path, l^*, increases, the width of the intensity cone decreases.

3 Experimental Arrangement

3.1 General Principles

There are two main technical challenges that need to be considered: separating the incident and scattered light, and achieving adequate angular resolution. In addition the light detector is a critical element.

Beam separation

It is not possible to observe light scattered directly backwards from a sample in a straightforward manner, since the detector would interfere with the laser beam. Therefore an essential component of any CBS setup is a "beam-splitter." This consists of a partially reflecting surface that passes some of the light (generally about 50%) while reflecting the remainder. If the partially-reflective surface is inclined at 45°to the original beam direction, the resulting sub-beams will be orthogonal.

Figure 3 [new schematic figure of beam splitter with intensities] shows how the beam splitter allows one to separate the light incident on the sample from the back-scattered light. ETC.

Achieving high angular resolution

Even tho laser beam seems to have very low divergence, in reality the typical divergence of 1 mR or so exceeds that required angular resolutuon. According to Gaussian optics, product of a divergence and diameter is a constant dependant only the wavelength (formula).

Therefore ...

Now discuss the lens ... with figure. maps the light rays that arrive from a particular direction (NOT a particualr point!) to a single point. maps angle to position.

Light detector

Scanning an aperture versus collecting an image.

3.2 Specific Components

Figure 4 shows the overall arrangement, which includes a linear polarizer , beam dump ... in addition to the components mentioned above. In this section we discuss the details of all of the specific components that were employed.

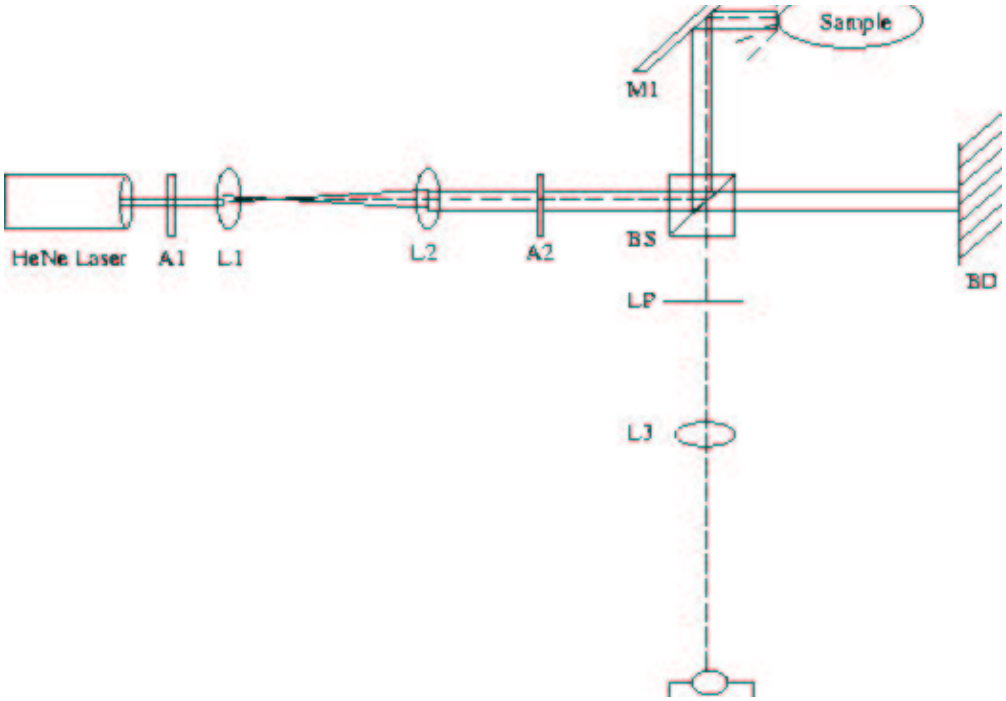

Figure 3: This is the basic schematic representation of the configuration I used for conducting my experiments. A1 and A2 represent the apertures used in the setup to block scattered light from the lenses. L1, L2 and L3 are convex lenses available from any ThorLabs Lens Kit with focal lengths of $2.54, 15$ and $20cm$, respectively. BS represents the beamsplitter, BD the beam dump, M1 the mirror that reflected the light onto the surface of the sample, and LP is the linear polarizer held orthogonal to the polarization incident on the sample to block out singly scattered light.

Laser

Beam expander

The laser beam was expanded to a beam waist of approximately 6 mm diameter, or six times the original waist, by using two convex lenses with focal lengths 2.54 and 15 cm, respectively, separated by the sum of their focal lengths. The collimation was checked by comparing the size of the beam immediately after the collimator with the size of the beam after it had

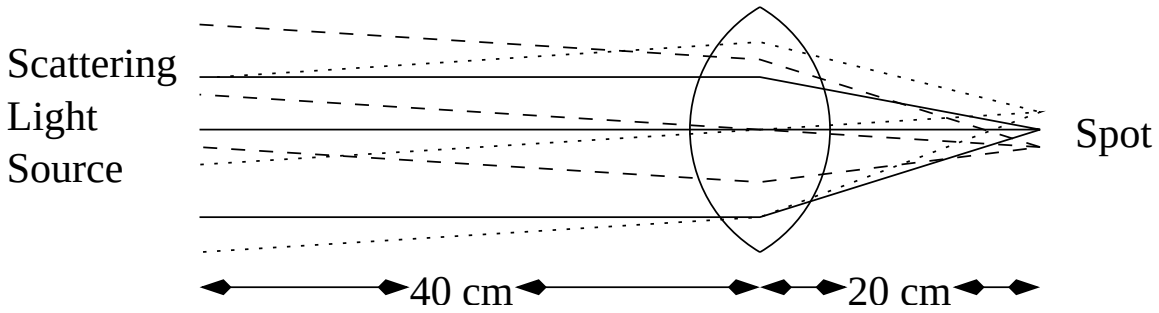

Figure 4: As light scattered to different angles enters the lens, it is focused to a point on the detection mechanism. Light from the area of interest creates a spot that can be detected by the CCD camera. In this setup, the size of the lens is a limiting factor to the amount of data that can be acquired since, as light which does not hit the lens is lost.

travelled a distance of about 5 m across the lab. A mirror was used to bring the beam back near the point of origin, so that the two beam spots could be compared "side by side."

Beamsplitter

The beam-splitter we used ... In this experimental setup, a 50:50 non-polarizing, anti-reflection coated cube beamsplitter was used to spearate teh beam into a probing beam and a free beam. Many past setups recommend the use of a glass beamsplitter with a slight wedge, in order to get rid of internal reflections from the anti-reflection coatings and scattering from the glue which holds a cube beam splitter together together. However, one was not available. In any case, a cube beamsplitter rotated slightly around its senter should prevent any internal reflections from reaching the exact backscattering direction (FIGURE?????).

Beam dump

A high-quality beam dump is essential since any light from the free beam scattered back could produce artifacts and interfere the results. The free beam was carefully dumped using polarizing filters and egg-crates. The beam dump was tested by dumping both the probing beam and free beam so that a black image was observed. More expensive beam dumps include stacks of razor blades or specially coated glass which localize light. These could allow for an easier and more efficient way to get rid of unwanted light, however for the

purposes of the experiment, the beam dump was sufficiently effective.

A mirror was used to shine the probing beam at a vertical angle onto the samples, preventing reflections from the face of a container. Scattered light from the specular reflection of the probing beam off the surface of the sample was not strong enough to effect the results.

CCD camera NOT cooled.

A relatively low cost (less than $1000) Electrim EDC-1000N computerized CCD camera with a 652 by 494 pixel array was used as the detection mechanism. Each pixel had an angular resolution of about 37 microradians as determined by the size of the pixel and the focal length of the lens. The camera took 50 frames in Multiple Frame Acquisition (MFA) mode, and averaged the data using a built-in software function to smooth out any specular background. The camera gain and bias values were adjusted until a clear picture was visible, and then remained constant during experimentation. Gain and bias are camera settings which help increase contrast and correct for some background noise in the input signal.

Sample and sample holder

3.3 Setup Procedures

The experimentation was carried out in a darkened, and a black cloth was used to create a sort of tunnel for the light in front of the CCD element. The software for the camera allowed the exportation of TIFF images of the exposures, which were then analyzed using NIH Scion Imaging Software [9].

Finding backscatter direction

Keeping components clean

Minimizing stray light

4 Analysis Procedures and Results

Software for the computerized CCD camera element exported camera exposures as raw TIFF images. (See Figure 4 for a colorized image of an intensity cone observed by the CCD camera.) The yellow area in the photograph represents the more intense light detected by the camera, whereas the blue areas represent the background scattered light. The exported

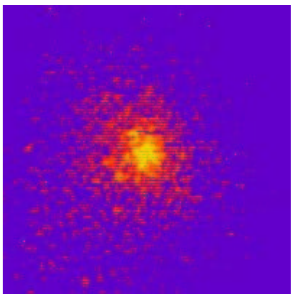

Figure 5: This is an image of a CBS cone observed from a $40ml$ sample of 1% milk. It was colorized using Scion Imaging software, and shows a clear enhancement about the center (180°).

TIFF images were loaded into NIH Scion Imaging Software. The image was colorized in order to determine the location of the intensity maximum more easily than in a black and white photograph, and vertical and horizontal cross-sections were taken through the center of the intensity cone. These cross-sections were then averaged about the center, which was deemed to be the common maximum value in the cross-sections of the intensity profile, in order to smooth out irregularities. These irregularities included pixel fluctuations, light trails, oscillations in the data due to a high gain setting, and possible bad pixels.

The CBS profiles for whole milk and skim milk are graphed in Figure 4. The data was fit with the intensity profile lineshape equation stated in Section 2.2. After a few iterations, the χ^2/N (where N represents the degrees of freedom for the fits) values for the fits were reduced to approximately 5. The results show that the experimental configuration was indeed able to detect CBS cones of varying Full-Widths at Half-Maximum (FWHM), and that l^* increases with the concentration of fat in the milk as expected. There are a few artifacts visible in the results, and they could be due to background light in the lab as well as reflections from the surface of the table or optical components. Although the components were aligned to get rid of as many of the reflections as possible, there could have been some minor reflections that contributed to these results causing the artifacts and 'hairy' appearance of the graphs. Another interesting feature of these results is the fact that the enhancement factor for the skim milk seems to be greater than the enhancement factor for the whole milk. This could be a result of the enhanced scattering coefficient of whole milk, which has a smaller l^*.

The exported images were shown to be caused by coherent backscattering and not some

other phenomenon, because when the detection mechanism was moved to an angle away from 180 °, the intensity profile changed and the cone disappeared.

As expected, the observed enhancement factors did not reach 2. Theory and past experimentation predict that in the linear polarization channels, enhancement factors of approximately 1.4 - 1.8 are expected for milk samples [2]. A quarter-wave plate, or a component which circularly polarizes light, is necessary in order to see the enhancement factor of two in the Helicity preserving channel ($H\|H$), where all of the singly scattered light and reflected is eliminated, and only the multiply scattered light is analyzed (source for this statement currently missing********). The unavailability of an anti-reflection coated in the lab prevented me from using it in my experimental setup, and when I tried a regular quarter-wave plate, reflections from the front and back surfaces of the plate lead to interference fringes. When it was placed perpendicular to the camera, too much light reflected back from the surface to be able to detect any CBS effect.

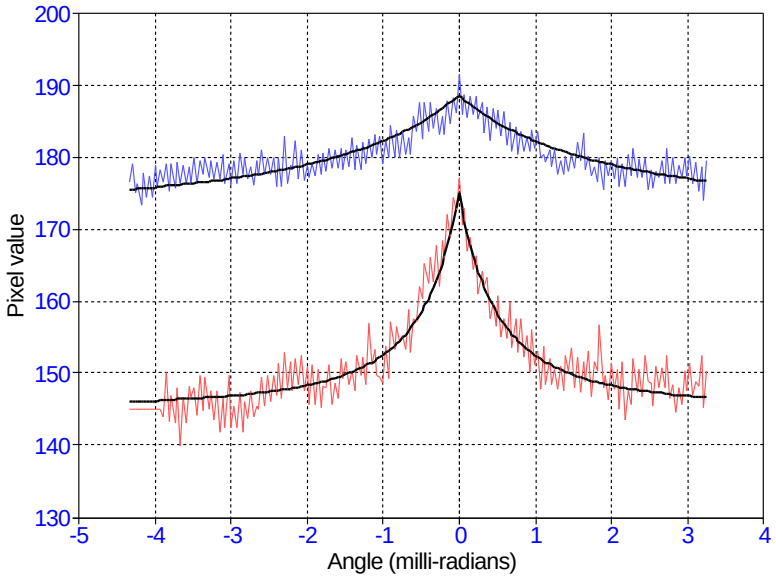

Figure 6: This graph shows the normalized profile plots of two different samples of milk, skim milk (red), and whole milk (blue) against the backscattering angle in terms of the observed pixel values by the CCD element. The wider Full Width at Half-Maximum (FWHM) of the whole milk suggests that the mean-free path length (l^*) of the photons scattering inside the milk is smaller than that of skim milk.

5 Discussion

The fact that there was slightly visible scattered light from the glued center of the cube beamsplitter lead to a lot of skepticism about whether the CBS cones could be observed.

Also, the CCD element was not cooled. A cooled CCD is far more expensive however, it is more accurate in measuring low level signals. In a normal non-cooled CCD camera such as the one used, there is a much greater probability that random pixels could be much more sensitive to light than others and lead to odd hot-spots in the exported images. There is also the question of the maximum resolution of the CCD element. There was only so much of an angular difference that the camera could detect - when the observed intensity spikes were expected to change only slightly between samples of milk, it was difficult to detect any change at all between them.

Another limitation of the current setup is that it is only currently possible to detect light scattered in the linear orthogonal polarization channel ($V \perp V$), since this orthogonal situation of the linear polarizer in the experimental configuration helps to block a lot of the light scattered from the center of the beamsplitter. Replacing the beamsplitter with a wedge-beamsplitter should remove most of these reflections and scattered light, and getting a higher quality linear polarizer could prevent some scattering from the polarizer itself. Also, the addition of an anti-reflection coated quarter-wave plate or another quarter-wave plate would allow for detection in the helicity channels ($H \| H$ and $H \perp H$).

6 Future Work

6.1 Polarization Channels

A major goal to extend the experimental configuration is to achieve detection in other polarization channels in order to observe the effect of polarization on coherent backscattering. This was not accomplished in the current setup, because an anti-reflection coated quarter-wave plate was not available, and a linear polarizer was positioned orthogonal to the polarization of the laser in order to block out scattered and reflected light from the beamsplitter. Changing the beamsplitter and adding another quarterwave plate to the experimental setup will

allow us to observe the light scattered in all four possible polarization channels, the linear polarization preserving channel ($V \| V$), the linear orthogonal polarization channel ($V \perp V$), the helicity preserving channel ($H \| H$), and the helicity orthogonal channel ($H \perp H$).

6.2 Data Analysis Methods

Using a CCD camera to export images of coherent backscattering intensity profiles provides us with a tremendous amount of information. By taking only vertical and horizontal cross-sections, we lose much of the data gathered. An interesting extension to the data analysis techniques would be to write an application which could determine the center of the CBS intensity spike in an exported TIFF image, and then use concentric circles outward from this centerpoint to determine the intensity profile. This would probably yield smoother data, and allow for a more efficient system of automatically determining the profile.

6.3 Future Experiments

The main purpose of the setup was to develop it in order to be able to apply it to future laboratory experiments. Some experiments involving coherent backscattering could be to use a magneto-optical trap in conjunction with the CBS setup in order to observe the CBS effect from ultracold atoms in order to understand how they scatter light. The setup can also be used to characterize complex media, such as biological tissue, photonic crystals, colloidal suspensions and densely packed random media by their optical properties.

7 Conclusion

One aim of this study was to observe coherent backscattering using a simplified method and experimental setup. Various issues were resolved by using low-cost optical components, and CBS intensity spikes were observed from samples of ordinary milk. A theoretical fit to the observations helped to characterize the samples by their optical properties such as the root-mean-free scattering path length. Various future extensions to the method and experimental configuration, and applications of the developed method were explored.

References

[1] Y. Kuga, A. Ishimaru, "Retro reflection from a Dense Distribution of Theoretical Particles," J. Opt. Soc. Am. A **1**, 831-835 (1984).

[2] S. A. Ramakrishna, K.D. Rao, "Estimation of light transport parameters in biological media using coherent backscattering," Pramana J. Phys. Vol. **54**, No. 2, 255-267 (February 2000).

[3] Albada, M. van and Lagendijk, A., "Observation of Weak Localization of Light in a Random Medium, Phys. Rev. Lett. 55, 2692-2695 (1985).

[4] Corey, R., Kissner M., Saulnier P. "Coherent Backscattering of Light" American Journal of Physics. Volume 63, 6. June 1995.

[5] A.F. Koenderink, M. Megens, G. van Soest, W.L. Vos, and A. Lagendijk Enhanced backscattering from photonic crystals. Phys. Lett. A 268, 104-111 (2000)

[6] Labeyrie G. et al. "Observation of coherent backscattering of light by cold atoms" Journal of Optics B. Opt. 2 (2000) 672-685

[7] Liang, S., and M.I. Mishchenko 1997. Calculations of the soil hot-spot effect using the coherent backscattering theory. Remote Sensing Environ. 60, 163-173, doi:10.1016/S0034-4257(96)00179-4.

[8] Mishchenko, M.I. 1993. On the nature of the polarization opposition effect exhibited by Saturn's rings. Astrophys. J. 411, 351-361.

[9] Scion Imaging Software is

[10] THESIS.

[11] Wiersma, D.S., Bartolini, P., Lagendijk, A., and Righini, R., Localization of Light in a disordered medium, Nature 390, 671 (1997).

[12] S. A. Ramakrishna, private communication, September 2003.